Appl. Phys. B 75, 377–383 (2002)
DOI: 10.1007/s00340-002-0987-4

Applied Physics B
Lasers and Optics

A. ROMANN
M.W. SIGRIST✉

Photoacoustic gas sensing employing fundamental and frequency-doubled radiation of a continuously tunable high-pressure CO_2 laser

Swiss Federal Institute of Technology (ETH), Institute of Quantum Electronics, Hönggerberg, 8093 Zürich, Switzerland

Received: 30 April 2002/Revised version: 10 June 2002
Published online: 2 September 2002 •

ABSTRACT We present the first photoacoustic spectrometer for gas sensing employing both the fundamental and the frequency-doubled radiation of a continuously tunable high-pressure CO_2 laser with room temperature operation. A quasi-phase-matched diffusion-bonded GaAs crystal is used in the system for second-harmonic generation. A pulsed photoacoustic detection scheme with a non-resonant cell, equipped with an 80-microphone array, is employed. The wide continuous tuning range in the fundamental (9.2–10.7 μm) and the frequency-doubled (4.6–5.35 μm) regimes, together with the narrow linewidth of 540 MHz (0.018 cm^{-1}) for the 10-μm region and of 1050 MHz (0.0315 cm^{-1}) for the 5-μm region, allow the measurement of gas mixtures, individual species and isotope discrimination. This is illustrated with measurements on NO and CO_2. The measured isotope ratio $^{15}NO/^{14}NO = (3.58 \pm 0.55) \times 10^{-3}$ agrees well with the literature (3.700×10^{-3}) and demonstrates the good selectivity of the system.

PACS 42.55.Lt; 42.62.F; 42.65.Ky; 42.68.Ca; 94.10.Gb; 07.07.Df

1 Introduction

Spectroscopic studies on gases have contributed to the understanding of the fundamental properties of gaseous compounds. In more recent years, spectroscopy has gained in importance as a non-contact method for a number of applications, such as environmental pollutant monitoring [1], industrial process control [2], plant physiology investigations [3], medical diagnostics by means of exhalation analysis [4] and crop and fruit storage [5]. Common to all these applications is the need for an accurate and time-saving technique to qualitatively and quantitatively record samples with high sensitivity and selectivity. To satisfy these requirements, well-established methods like mass spectrometry [6, 7] and gas chromatography [8] have been introduced. Both methods yield high sensitivity and selectivity but require some kind of sample preparation and hence lack time resolution. In addition, they are generally not as universally applicable to all kinds of compounds as optical spectroscopic schemes. Here, we focus on optical absorption-based methods which offer some distinct advantages, provided that certain elements of the sensing system, particularly the radiation source and the detection scheme, are carefully designed. High sensitivity, i.e. measurement of low concentrations, requires strong, i.e. fundamental, absorption features to be chosen. For many small organic and inorganic species, these lie in the infrared (IR) region between, say, 3700 cm^{-1} and 500 cm^{-1} (2.7–20 μm). A widely, and ideally, continuously tunable radiation source with sufficient power employed in this spectral region is therefore preferred and should be combined with a sensitive detection scheme. Several detection methods are in use today, such as long-path absorption, either as open-path, for example for fence monitoring, or in a multipass absorption cell [9, 10], cavity ring-down (CRD) [11] or photoacoustics (PA) [12, 13]. We apply PA detection, which offers some interesting features such as small cell volume, no requirement for highly reflecting mirrors and no need for a cooled IR detector. Since the PA signal is registered by a microphone, there is inherently no wavelength dependency and the same cell can be employed for different wavelength regions.

High selectivity is achieved by the use of a narrow-linewidth radiation source. This enables the sensing of a species in the presence of others, for example in multicomponent samples, or discriminating between isotopes. Lasers, with their inherent narrow linewidth, are thus ideal radiation sources for this purpose. Further requirements of gas sensing applications may include operation at room temperature, small sample volume, continuous real-time monitoring, a compact and rugged set-up and cost effectiveness and reliability for industrial use. Not all lasers available in this wavelength region of interest operate at room temperature. For example, lead-salt diode lasers require cryogenic temperatures if operated in single mode and continuous wave [14]. Thermoelectric cooling may be used for pulsed operation, but this consumes additional power and produces excessive heat. Furthermore, condensation of water may cause problems with cooled laser sources. The recent development of quantum cascade lasers (QCL) [15], with their tailored emission wavelengths and room- or near-room-temperature operation may become the preferred laser source for gas sensing and other applications in the future. At present, their tunability is limited to a few cm^{-1} which restricts their application to the detection of selected species rather than to the analysis of multicompo-

✉ Fax: +41-1/633-1077, E-mail: sigrist@iqe.phys.ethz.ch

nent mixtures. Hence, primary laser sources are not readily available throughout the whole region of interest in the mid-infrared (MIR) and far-infrared (FIR). Non-linear frequency conversion [16], for example difference frequency generation (DFG) [17] or the use of an optical parametric oscillator (OPO), is often employed to extend the accessible wavelength range. A wide selection of high-quality bulk and periodically poled non-linear optical materials [16, 18] is available and the list continues to grow.

To underline the importance of a narrow laser source in spectroscopic applications such as PA, long-path absorption and CRD, we discuss briefly two recent OPO designs beyond 5 μm as alternatives to our approach of frequency doubling a CO_2 laser. Shori et al. [19] report on a powerful OPO exceeding 10 mJ pulse energy at 6.1 μm, which makes it suitable as a source in a PA spectrometer. However, no information on the linewidth is given. Vodopyanov et al. [20] demonstrated an OPO with an etalon (Si plate) as the wavelength-selective element for narrowing the emission linewidth. Its wide emission range of 3.8–12.4 μm covered the fundamental molecular absorption regions of many species. However, the linewidth of about 0.4 cm^{-1} (12 GHz) of this free-running OPO was considerably larger than the width of a typical molecular absorption line at normal pressure, and was thus not adequate for PA or long-path absorption investigations on gaseous media at pressures of 1 bar and below. Also, CRD relies on a narrow linewidth for high spectral resolution. The typical cavity length is a few tens of centimetres. For example, in [11] the length was 0.255 m, which resulted in a spectral mode separation of about 590 MHz. Hence, several cavity modes are excited and the good spectral resolution would be lost without the application of further line-narrowing elements such as a high-finesse etalon with a wide free spectral range. It should be stressed that the CRD cavity and the line-narrowing etalon must be coupled to the laser emission wavelength, which we consider to be a costly effort.

Here, we describe a continuously tunable CO_2 laser whose fundamental (FUN) emission range has been extended by second-harmonic generation (SHG). Both the FUN (10 μm) and SHG (5 μm) radiations are applied to a non-resonant photoacoustic detection scheme. Since measurements employing this source in the FUN range have been discussed previously [21, 22], we concentrate here on the SHG region. Table 1 lists selected substances [23–27] with distinct absorption features accessible with our laser source. The list contains organic and inorganic species which have an impact in very diverse areas. In the following, the laser source, including the employed SHG crystal, is described first. Some key specifications and operating parameters are given. The PA detection scheme is discussed thereafter. PA spectroscopic measurements on selected gases illustrate the performance of the spectrometer and are also used to derive parameters such as linewidth in the SHG region and the pressure regime for the optimum PA signal.

2 Experimental set-up

The experimental set-up is depicted in Fig. 1. It comprises the pulsed CO_2 laser operated in the fundamental and the SHG regime, a photoacoustic detection scheme and data acquisition. The FUN emission ranges have been measured, while the SHG ranges have been calculated, but only the 10P branch has so far been experimentally verified. The CO_2 laser is a home-built continuously tunable high-pressure laser described in detail elsewhere [28]. Tuning and radiation characteristics are summarised in Tables 2 and 3. All SHG characteristics listed in Table 3 are deduced from measurements presented here. The linewidths of 540 MHz in the FUN and of 1050 MHz for the SHG are considerably smaller than a typical molecular absorption linewidth (≥ 0.1 cm^{-1} or 3 GHz) at atmospheric pressure. As shown on the set-up in Fig. 1, the pump laser is wavelength-tuned by rotating a flat mirror by a computer-controlled DC-drive. The metal

Species	FUN [10 μm] (cm^{-1})	SHG [5 μm] (cm^{-1})	Potential relevance
Acetaldehyde, CH_3CHO	1200–1060		Incomplete wood combustion, alcohol metabolism, fruit storage, higher plant respiration
Acetone, $(CH_3)_2CO$ (and other ketones)	950–930		Solvent, dairy cattle health, metabolic stress, cancer indicator, diabetes, blood sugar deficiency,
Ammonia, NH_3	970–920		Industrial processes, acid rain, refrigeration, volcanic gas, agriculture, fertiliser dispersal, kidney and liver disease
Arsine, AsH_3		2126	Semiconductor industries, chemical warfare
Bromomethane, CH_3Br	1035–930		Soil (pre-planting) fumigation
Carbon monoxide, CO		2200–2100	Combustion, neonatal jaundice, asthma, gastric liver, blood condition, haeme protein metabolism
Carbon dioxide, CO_2	1085–980	2076–2095	Combustion, greenhouse gas, volcanic gas, asthma, gastric liver, blood/lung gas-interchange
Carbonyl sulfide, COS		2080–2030	Volcanic gas, fumigant, fruit storage
Dimethyl ether, $(CH_3)_2O$	1000–930		Propellant, diesel fuel substitute
Ethanol, C_2H_5OH	1090–1020		Fuel substitute, alcohol metabolism, fruit storage
Ethylene, C_2H_4	950		Combustion, plant decay, plant hormone, fruit and vegetable ripening and storage
Nitric oxide, NO		1920–1870	Acid rain, smog, ozone formation, diabetes, cancer, anorexia, tuberculosis, amino acids
Water, H_2O		1980–1350	Natural respiration, humidity, industrial processes, semiconductor industries

TABLE 1 Selected absorbing species accessible with our laser source. The last column indicates their relevance in different areas

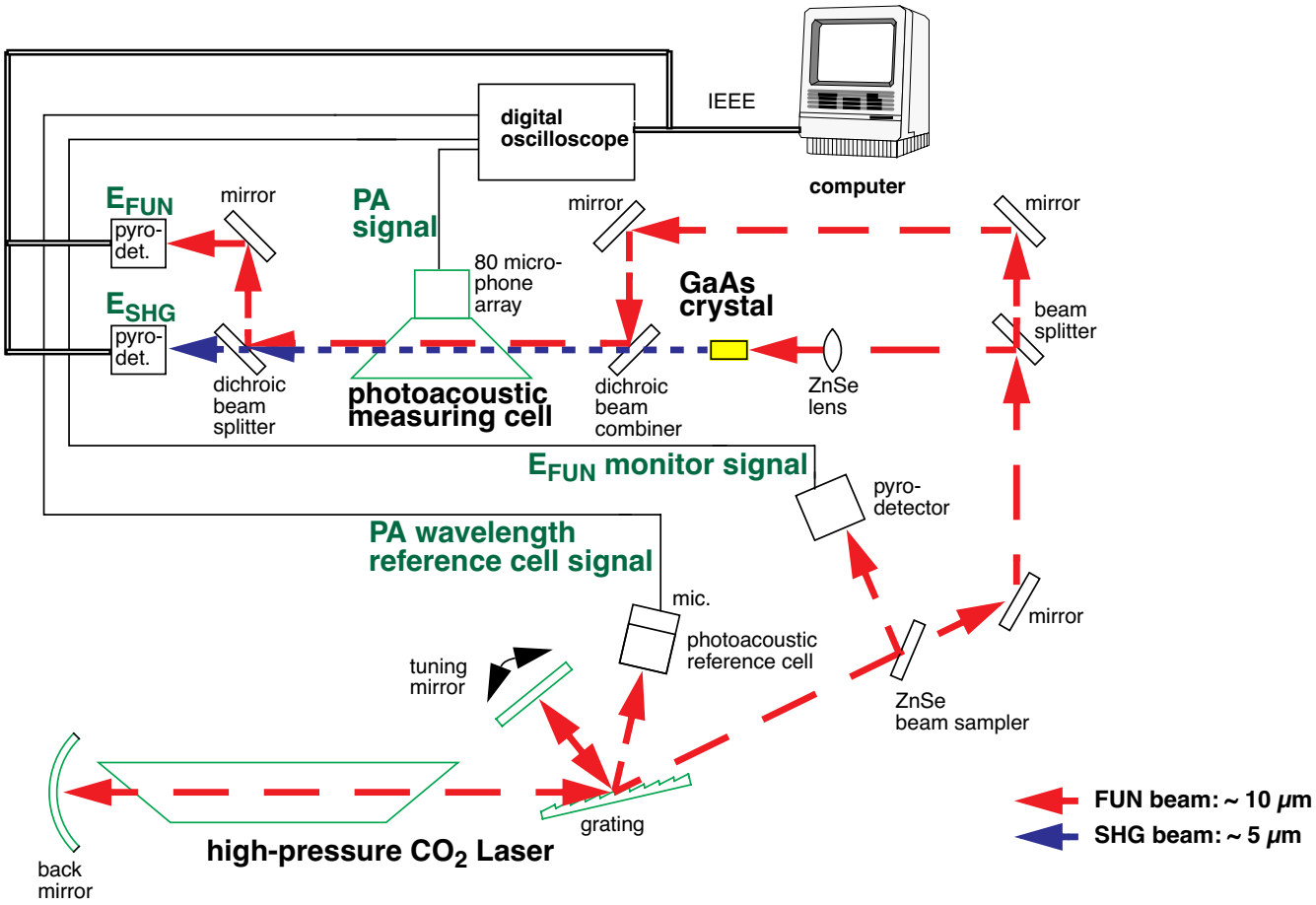

FIGURE 1 Photoacoustic spectrometer employing the frequency-doubled continuously tunable CO_2 laser and the 80-microphone-array measurement cell. FUN, fundamental; SHG, second-harmonic generation

TABLE 2 FUN (10 μm) and SHG (5 μm) tuning ranges

CO_2 laser branch	transition	FUN (10 μm) range (cm^{-1})	(μm)	SHG (5 μm) range (cm^{-1})	(μm)
10P	P(32)–P(8)	932.47–954.14	10.72–10.48	1864.94–1908.28	5.36–5.24
10R	R(6)–R(30)	965.88–981.81	10.35–10.19	1931.76–1963.62	5.18–5.09
9P	P(28)–P(8)	1038.89–1056.89	9.63–9.46	2077.78–2113.78	4.82–4.73
9R	R(4)–R(36)	1067.16–1087.69	9.37–9.19	2134.32–2175.38	4.69–4.60

TABLE 3 Characteristics of the fundamental and frequency-doubled continuously tunable high-pressure CO_2 laser

	FUN (10 μm) range	SHG (5 μm) range
Pulse energy	Max. 80 mJ, minimal 10 mJ throughout the tuning range	Max. 1 mJ, typically 0.04 to 0.4 mJ
Pulse repetition rate	1 Hz typically	Same as pump rate
Pulse length (FWHM)	140 ns	Not measured
Linewidth	0.018 cm^{-1} (540 MHz)	0.0315 cm^{-1} (1050 MHz)
Laser gas mixture	5% CO_2, 5% N_2, 90% He	Same as pump source
Operating pressure	10 bar typically	Same as pump source

diffraction grating is positioned in Littman configuration at an incident angle of 77°. It has 150 lines/mm and is blazed for 943.4 cm^{-1} (10.6 μm). The first-order reflection off the grating is reflected back and the zeroth order is coupled out. An additional reflection off the grating is used for emission-wavelength recording. This wavelength-tuning configuration results in a very narrow laser linewidth, well suited for applications in spectrometers.

The applied non-linear material was a diffusion-bonded periodically poled GaAs crystal [29]. GaAs has a large non-linear coefficient, is transparent in the range from 1 to 16 μm, features low absorption, has a high thermal conductivity, high average power capabilities and a high damage threshold. Hence, it compares favourably with well-known non-linear IR materials such as $AgGaSe_2$ [30, 31] and $ZnGeP_2$ [31, 32]. Table 4 lists some of the commonly used non-linear materials for CO_2-laser frequency conversion with the key parameters; the non-linear coefficient, transparency range and damage threshold. Apart from GaAs, $CdGeAs_2$ exhibits a very high figure of merit, but is not yet grown with sufficient optical

Non-linear optical material	Non-linear coefficient [10.6 μm] (pm/V)	Transparency range (μm)	Damage threshold (pulse duration at wavelength)
GaAs	$d_{14} \approx 90$	1–16	30 MW/cm^2 (90 ns at 10.6 μm)
$AgGaSe_2$	$d_{36} = 33$	0.71–19	10 MW/cm^2 (125 ns at 10.6 μm)
$CdGeAs_2$	$d_{36} = 235$	2.4–18	33 MW/cm^2 (150 ns at 10.6 μm)
GaSe	$d_{22} = 54.4$	0.62–20	30 MW/cm^2 (150 ns at 9.3 μm)
$ZnGeP_2$	$d_{36} = 75$	0.74–12	60 MW/cm^2 (100 ns at 10.6 μm)

TABLE 4 Selected non-linear optical materials [16, 18] used for frequency conversion of 10-μm radiation

quality for operation at room temperature [31]. However, reported non-linear coefficients d_{14} ($= d_{36}$) of GaAs for 10.6 μm vary significantly between 90 pm/V [33], 151 pm/V [34] and 368.7 pm/V [35]. Shoji et al. [36] list values in the NIR region which suggest a non-linear coefficient in the 10 μm region of approximately 90 pm/V. GaAs, a $\bar{4}3m$ crystal, is not birefringent, and thus periodically poled material has to be employed for quasi-phase-matching (QPM). Since GaAs is not ferroelectric, no technique such as electric field-poling in $LiNbO_3$ exists for inducing domain gratings in an already-grown crystal. The bonding of slabs [29] or recently developed thick-film-growth techniques [33], such as hydride-vapor phase epitaxy (HVPE) can be used to fabricate orientation-patterned GaAs crystals. The estimated figure of merit for first-order QPM for the employed crystal [29] is given by:

$$\frac{\left(d_{\mathrm{eff}}^{\mathrm{QPM}}\right)^2}{n_\omega^2 \cdot n_{2\omega}} = \frac{1}{n_\omega^2 \cdot n_{2\omega}} \cdot \left(\frac{2}{\pi} \cdot \frac{2}{\sqrt{3}} \cdot d_{36}\right)^2 \approx 124\ (\mathrm{pm/V})^2 \quad (1)$$

where n_ω and $n_{2\omega}$ denote the refractive indices at FUN and SHG wavelengths, respectively. The crystal employed here with overall dimensions of $2 \times 4 \times 5.6$ mm consists of 53 (110) GaAs plates of approximately 106 μm thickness, each for first-order quasi-phase-matching. Both faces are AR-coated for FUN and SHG wavelengths, but the coatings had already suffered when the crystal was received. As stated in [29], the conversion efficiency for this crystal is not equally high across the crystal face. Higher efficiency is obtained with better transmission in the centre along the optical axis. To avoid boundary effects, the pump beam was focused on the face centre. This favours safe operation rather than high conversion efficiency. Figure 2 shows the expected quadratic relation between the pump intensity I_ω (polarised along ⟨111⟩) [37] and the SHG beam intensity $I_{2\omega}$, given as:

$$I_{2\omega} \propto \frac{\left(d_{\mathrm{eff}}^{\mathrm{QPM}}\right)^2}{n_\omega^2 \cdot n_{2\omega}} \cdot (N \cdot l_\mathrm{c})^2 \cdot I_\omega^2 . \quad (2)$$

N is the (odd) number of domains and l_c is the coherence length. As Fig. 2 implies, we achieved SHG pulse energies E_{SHG} of up to 1 mJ, corresponding to an (external) energy conversion efficiency of 1% at a pump energy E_{FUN} of 80 mJ. A theoretical estimation (plane-wave non-depleted pump approximation) with the maximum applied pump intensity I_ω of 21.5 MW/cm^2 gives an external energy (flat-top pulse) conversion efficiency of 11.4%. Since the anti-reflection coating was damaged, it was ignored completely and Fresnel reflection was used. The crystal periodicity was assumed to be perfect. This estimation neglects the actual temporal pulse form exhibiting longitudinal mode beating, spatial intensity distribution of the TEM_{00} mode, limited crystal transparency of 60% and deviation from ideal periodicity, as well as focusing parameters. Hence, this estimation gives an upper limit and some parameters, needed for a more sophisticated theoretical approach, vary considerably from pulse to pulse, as is evident from Fig. 2. It should be noted that the actual conversion efficiency and hence the achievable SHG pulse energy is limited by the damage threshold of the crystal of 30 MW/cm^2 [29].

As shown in Fig. 1 above, a compact PA reference cell filled with 200 mbar CO_2 was employed for wavelength calibration of the spectrometer. An angle-tunable beam sampler made of an uncoated ZnSe flat coupled out a small fraction of the FUN energy for recording of the pulse energy. Two gold-coated copper mirrors were applied for beam guiding. An AR-coated ZnSe meniscus lens with 10″-focal length collimated the 2.3-mm-diameter FUN beam onto the non-linear crystal. An uncoated 2-mm-thick sapphire flat with a cut-off

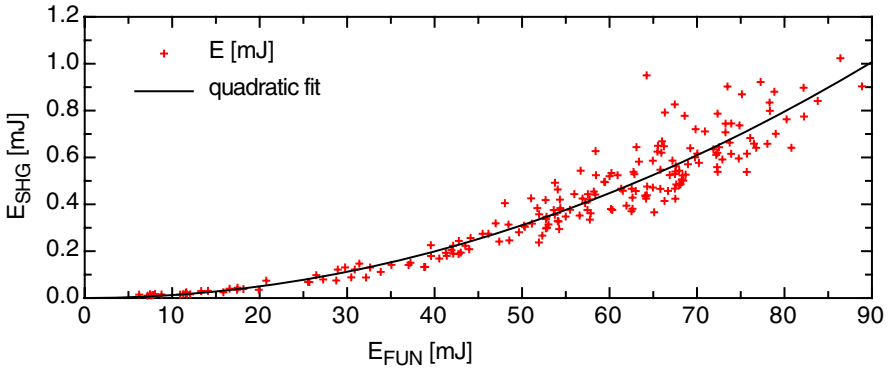

FIGURE 2 Measured second-harmonic generation pulse energy E_{SHG} vs. fundamental pulse energy E_{FUN}. The *solid line* indicates the quadratic fit according to (2). The energy conversion efficiency is 1% at a pump energy of 80 mJ

wavelength of 5.5 μm in Brewster-arrangement for SHG radiation filtered out the FUN pulse.

The PA measuring cell required careful design. The generated PA signal $S(\lambda, t) \propto I(\lambda, t) \cdot N \cdot \sigma(\lambda)$ depends linearly on the intensity of the incident radiation $I(\lambda, t)$, the number density N of absorbing molecules and their cross section $\sigma(\lambda)$. The PA signal is affected by noise originating from window heating, turbulent gas flow, microphone and electric noise. In the pulse regime, window-heating signals can simply be discriminated in the data acquisition process by time gating. The actual PA signal amplitude is determined as the difference between the peak of the first oscillation and the baseline before the PA signal. The baseline is assumed to remain unchanged in the time the two values are recorded. All figures feature such single events.

Our PA cell [38] employed an 80-microphone array (Knowles BK 1751 electret microphones). It was sealed with BaF_2 Brewster windows and operated in stop and flow modes at and below atmospheric pressure. The small gas volume of 0.18 l, together with a turbulence-free flow rate of up to 0.7 l/min, resulted in a time constant of a few seconds for a complete gas exchange. The battery-powered bandwidth-limited low-noise preamplifier (bandpass: centre 15 kHz, width 10 kHz) was built into the cell for noise reduction. Additional high- and low-pass filters suppressed broadband and high-frequency noise generated by the laser discharge. A calibrated pyroelectric energy meter (Ophir LaserStar with measuring head PE 10-SH) recorded the SHG pulse energy, which normalised the measured PA signal. The PA signal and the FUN monitor signals were acquired by a digital oscilloscope. The fast and sensitive pyroelectric detector (not shown in Fig. 1), facing towards the grating, generated the trigger signal for the digital oscilloscope. A computer controlled the experiment and stored the acquired data. A gas mixing unit (not shown in Fig. 1) with mass-flow controllers was used for gas sample preparation.

3 Measurements and results

The PA cell response was deduced from measurements on NO diluted in nitrogen for total pressures ranging from 58 mbar to 858 mbar. The solid line in Fig. 3 represents the pressure-dependent absorbance on the basis of HITRAN data [23]. The PA signal is nearly constant for total gas pressures from near atmospheric pressure down to 400 mbar, but decreases strongly for pressures below 400 mbar. For a pressure of 200 mbar, the signal has halved. The deviation of the PA signal from the absorbance shows a similar dependence as discussed above, it is also more pronounced at gas pressures below 400 mbar. Both effects are attributed to three causes, namely the responsivity of the microphone employed here, the number density of the absorbing species and the overlap of the laser and absorption lines. The microphone responsivity [39] depends on pressure and is an inherent property of the microphone. The number density of the absorbing species scales linearly with pressure, although its concentration, i.e. 1% NO diluted in N_2, was constant in our measurement. With lowering the pressure, the linewidth of the absorption line is reduced, with contributions from both Doppler and pressure broadening. In this case, the amount of absorbed radiation is determined by the convolution of the (broad) laser linewidth and the (narrow) absorption line profile. This effect will hence reduce the observed energy-normalised PA signal.

Despite this drop in sensitivity, it should be emphasised that PA measurements at lower pressures may still be advantageous because absorption features become more distinct, for example in cases of multicomponent samples which require high selectivity to be analysed. This approach is, however, limited by the available laser linewidth.

NO buffered in N_2 was measured at concentrations of 493 ppmV and 1% at various pressures and wavelengths at room temperature in stop-flow mode. Figure 4 depicts a measurement of 493 ppmV NO, buffered in N_2 at room temperature and normal pressure. HITRAN data [23] for NO in the range of the frequency-doubled 10P branch of the CO_2 laser are given in Fig. 4a. The Q-branch is shown in Fig. 4b.

Another important issue is the $^{15}N/^{14}N$ isotope ratio, which can be determined with our system. A non-invasive spectroscopic detection of ^{15}N (often together with $^{13}CO_2$) would provide a risk-free alternative to radioactive tracers in medical diagnostics, for example, to study nitrogen metabolism in humans, for example collagen turnover, amino acids or Helicobacter pylori [40]. The detection of the $^{15}N/^{13}C$ isotope ratio from N_2 and CO_2 mass-spectrometric measurements may be difficult. There is relatively low nitrogen in organic compounds, for example amino acids contain 11-times more carbon than nitrogen. N_2 and CO (from incomplete combustion) produce an isobaric interference at $m/z =$

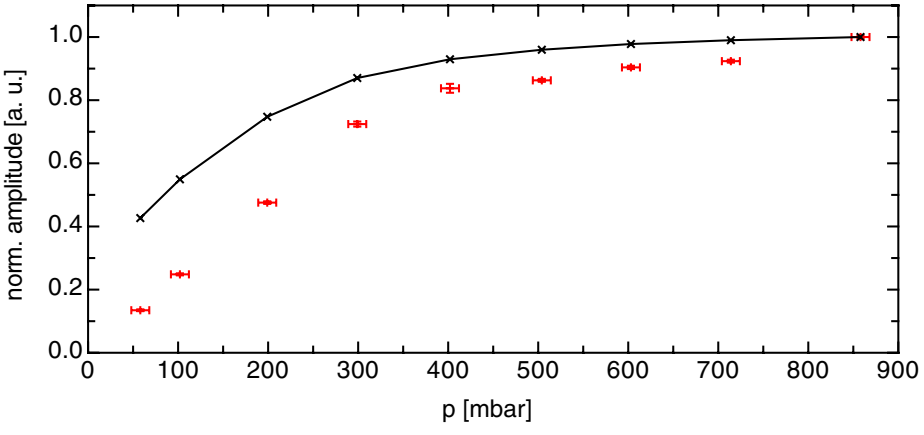

FIGURE 3 Measured microphone signal for 1% NO diluted in nitrogen vs. total gas pressure around 1881 cm^{-1}. HITRAN reference data (*solid line*) indicates the decrease in absorbance. The experimental and HITRAN data are normalised to coincide at a pressure of 858 mbar. The deviation between measured data and HITRAN data is attributed to the pressure-dependent microphone responsivity, the reduction in the number of absorbing molecules and the reduction in the linewidth overlap between the absorption and laser lines

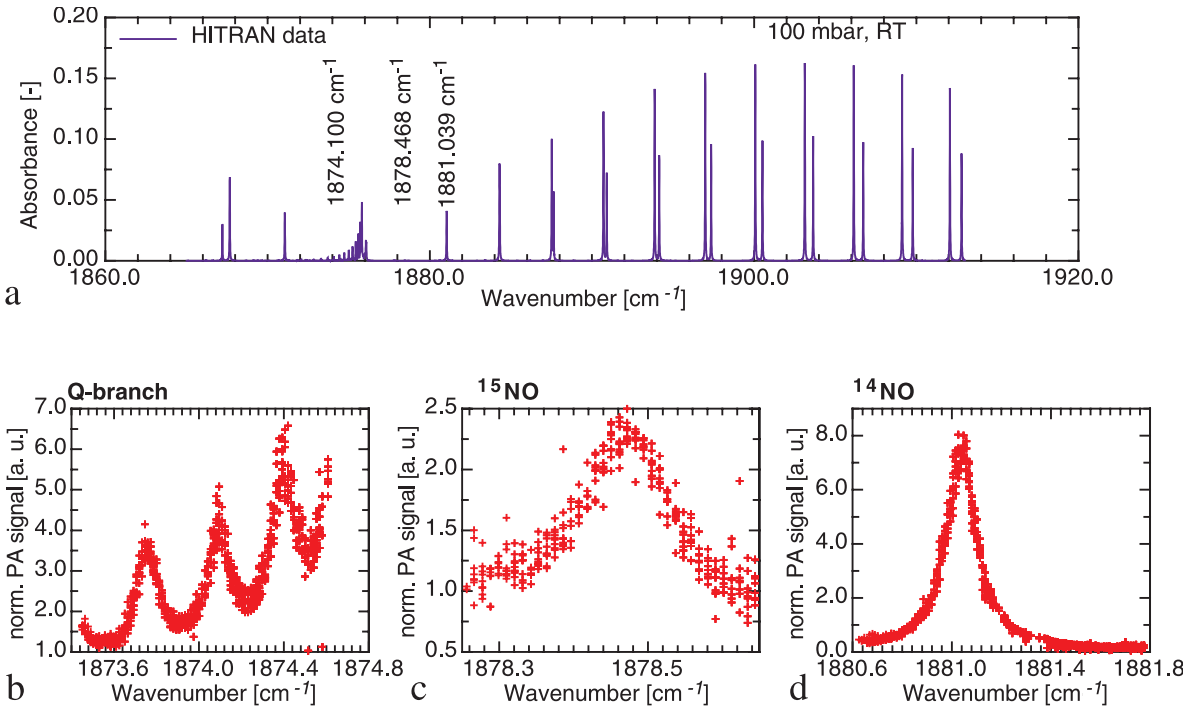

FIGURE 4 Normalised PA spectrum of 493 ppmV NO buffered in N_2. **a** HITRAN spectrum (at 100 mbar) as line position reference; the three wavelengths indicated refer to the measurements below in **b** to **d**, all taken at atmospheric pressure and room temperature (RT). **b** Q-branch measurement around 1874.1 cm^{-1}. **c** Measurement of ^{15}NO around 1878.468 cm^{-1}. **d** Measurement of ^{14}NO around 1881.039 cm^{-1}

28 (mass-to-charge-ratio). We derived the $^{15}NO/\,^{14}NO$ isotope ratio by measuring ^{14}NO at 1881.039 cm^{-1} in Fig. 4c and ^{15}NO at 1878.468 cm^{-1} in Fig. 4d. The resulting value of $(3.58 \pm 0.55) \times 10^{-3}$ is in good agreement with literature data of 3.700×10^{-3} [41]. From Fig. 4, it should be noted that the precision of the isotope measurement could be substantially improved by measuring at an absorption line in the 1903 cm^{-1} region and also if higher concentrations of NO were analysed.

The absorption line of NO at 1881.039 cm^{-1} recorded at a pressure of 58 mbar was used for deriving the laser linewidth in the SHG regime. Taking a Gaussian absorption profile (for simplicity) and a Gaussian laser line profile, a value of 0.0315 cm^{-1} (1050 MHz) was deduced, as listed in Table 3.

Figure 5 shows a measurement of another relevant gas, namely CO_2. This compound is listed in Table 1, although the SHG wavelengths are outside the strong absorption region of CO_2. Nevertheless, CO_2 monitoring is feasible as the experimental data that were recorded at 249 mbar of pure CO_2 and their comparison with HITRAN data [23] demonstrate.

The detection limits for NO and CO_2 for a signal-to-noise-ratio (*SNR*) of 3 were derived from measurements of 493 ppmV NO diluted in N_2 recorded at 1881.039 cm^{-1} and from pure CO_2 recorded at 1899.115 cm^{-1}. To determine the detection limit, an absorption line was scanned and the line profile was fitted. The amplitude of the fitted function was then compared to three-times the standard deviation of the baseline ($SNR = 3$). For each wavelength position of the scan, 10 data points were collected, which corresponded to a measuring time of 10 s. The total measurement time for the spectrum shown in Fig. 4d for example, with wavelength steps of 7.5×10^{-3} cm^{-1}, was about 40 min.

The rather high detection limits of 42 ppmV for NO and of 2.55% for CO_2 were due to the low pulse energies of $E_{SHG} \leq 1$ mJ presently available in the 5 μm wavelength range, the

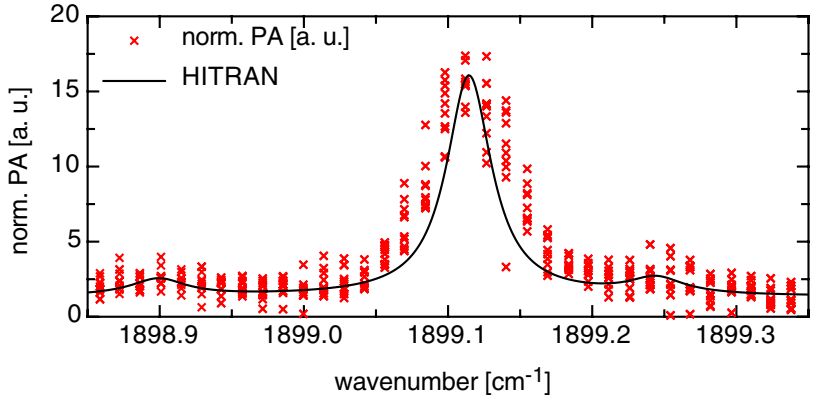

FIGURE 5 Normalised PA CO_2 spectrum measured at a pressure of 249 mbar and room temperature around 1899.115 cm^{-1}, compared with HITRAN data [23]

fact that only non-resonant PA detection was feasible at the small pulse repetition rates involved, and, in the case of CO_2, the small absorption cross section outside the fundamental region.

4 Conclusions

Our photoacoustic spectrometer, based on a fundamental and frequency-doubled high-pressure CO_2 laser, features a wide and continuous tuning range in the 10-μm and 5-μm regimes and room temperature operation. It is well suited for spectroscopic investigations, with strong fundamental absorption lines of various species falling within these two wavelength regions. Its narrow linewidth in both regimes, combined with the fast access of a specific wavelength, enables both selective multicomponent trace gas monitoring and also fundamental spectroscopic studies on molecules, like the determination of isotope ratios. The wide emission wavelength ranges favour a photoacoustic detection scheme, with its inherent wavelength-independent response. The current rather low sensitivity of the system could be improved by applying a multipass PA arrangement [42] or by increasing the SHG pulse energies with the implementation of a longer non-linear crystal. It should be noted, however, that even the current detection limits are of interest, for example in industrial gas monitoring. As example, the maximum permissible work place concentration for NO (25 ppmV (30 mg/cm^3) in Switzerland) is within reach of the present performance.

Because of the inherent low pulse repetition rate, a high-pressure CO_2 laser is not suitable for fast scans over extended wavelength ranges, which would be necessary when investigating gas samples which may not be stable over time. Quantum cascade lasers (QCL) with tailored emission wavelengths in combination with PA detection [43–45] could represent a suitable alternative in such cases. In the future, external cavity QCLs with extended tuning range, narrow linewidth and average power greater than 10 mW at room temperature would in fact provide an excellent spectroscopic tool for numerous applications.

ACKNOWLEDGEMENTS We acknowledge the support by the Swiss National Science Foundation, the Alliance for Global Sustainability (AGS, AVINA Funds) and ETH Zurich. The GaAs crystal has been kindly supplied by L. Becouran and E. Lallier, Thomson-CSF/LCR, Orsay, France.

REFERENCES

1 J. Slania: *Biosphere Atmosphere Exchange of Pollutants and Trace Substances* (Springer, Berlin 1997)
2 T. Hodges, G.E. Scace, J.A. Silver: Appl. Opt. **40**, 829 (2001)
3 R.R. Wise, A.W. Nylor: Plant. Physiol. **83**, 272 (1987)
4 L.R. Narasimhan, W. Goodman, C.K.N. Patel: Proc. Natl. Acad. Sci. **98**, 4621 (2001)
5 J. Oomens, H. Zuckermann, S. Persijn, D.H. Parker, F.J.M. Harren: Appl. Phys. B **67**, 459 (1998)
6 D. Bassi, P. Tosi, R. Schloegl: J. Vac. Sci. Techol. A **16**, 114 (1998)
7 W. Lindinger, A. Hansel, A. Jordan: Int. J. Mass Spectrom. Ion Process. **173**, 191 (1998)
8 K. Robards, P.R. Haddad, P.E. Jackson: *Principles and Practice of Modern Chromatographic Methods*, 1st edn. (Academic Press, London 1994)
9 M. Seiter, M.W. Sigrist: Appl. Opt. **38**, 4691 (1999)
10 D. Richter, D.G. Lancaster, F.K. Tittel: Appl. Opt. **39**, 4444 (2000)
11 Y. He, B.J. Orr: Chem. Phys. Lett. **319**, 131 (2000)
12 M.W. Sigrist: 'Air monitoring by laser photoacoustic spectroscopy'. In: *Air Monitoring by Spectroscopic Techniques*, Vol. 127, *Chemical Analysis Series*, ed. by M.W. Sigrist (Wiley, New York 1994) Chapt. 4
13 A. Miklós, P. Hess, Z. Bozóki: Rev. Sci. Instrum. **72**, 1937 (2001)
14 P. Werle: Spectrochim. Acta A **54**, 197 (1998)
15 J. Faist, F. Capasso, D.L. Sivco, C. Sirtori, A.L. Hutchinson, A.Y. Cho: Science **264**, 553 (1994)
16 R.L. Sutherland: *Handbook of Non-Linear Optics* (Marcel Dekker, Basel New York 1996)
17 H.D. Kronfeldt, G. Basar, B. Sumpf: JOSA B **13**, 1859 (1996)
18 V.G. Dmitriev, G.G. Gurzadyan, D.N. Nikogosyan: *Handbook of Non-Linear Optical Crystals, Springer Series in Opt. Sciences*, Vol. 64, 3rd rev. edn. (Springer Verlag, Berlin 1999)
19 R.K. Shori, O.M. Stafsudd, N.S. Prasad, G. Catella: Opt. Soc. Am. TOPS **46**, 179 (2000)
20 K.L. Vodopyanov, F. Ganikhanov, J.P. Maffetone, I. Zwieback, W. Ruderman: Opt. Lett. **25**, 841 (2000)
21 I.G. Calasso, V. Funtov, M.W. Sigrist: Appl. Opt. **36**, 3212 (1997)
22 P. Repond, M.W. Sigrist: Appl. Opt. **35**, 4065 (1996)
23 L.S. Rothman, C.P. Rinsland, A. Goldman, S.T. Massie, D.P. Edwards, J.M. Flaud, A. Perrin, C. Camy-Peyret, V. Dana, J.Y. Mandin, J. Schroeder, A. McCann, R.R. Gamache, R.B. Wattson, K. Yoshino, K.V. Chance, K.W. Jucks, L.R. Brown, V. Nemtchinov, P. Varanasi: J. Quant. Spectrosc. Radiat. Transfer **60**, 665 (1998)
24 QA Soft – 96: *Database and Quantitative Analysis Programs for Measurement of Gases* (Infrared Analysis Inc., Anaheim 1996)
25 NIST: *Chemistry WebBook*, *Standard Reference Database 69*, http://webbook.nist.gov/chemistry/
26 NIST: *Quantitative Infrared Database*, *Standard Reference Database 79*, http://www.nist.gov/srd/nist79.htm
27 EPA: *AEDC/EPA spectral database*, http://www.epa.gov/ttn/emc/ftir/data.html
28 P. Repond, M.W. Sigrist: IEEE J. Quantum Electron. **QE-32**, 1549 (1996)
29 E. Lallier, M. Brevignon, J. Lehoux: Opt. Lett. **23**, 1511 (1998)
30 E. Tanaka, K. Kato: Appl. Opt. **37**, 561 (1998)
31 M.M. Tilleman, A. Englander: Opt. Eng. **39**, 758 (2000)
32 S.Y. Tochitsky, V.O. Petukhov, V.A. Gorobets, V.V. Churakov, V.N. Jakimovich: Appl. Opt. **36**, 1882 (1997)
33 L.A. Eyres, P.J. Tourreau, T.J. Pinguet, C.B. Ebert, J.S. Harris, M.M. Fejer, L. Becouarn, B. Gerard, E. Lallier: Appl. Phys. Lett. **79**, 904 (2001)
34 M.M. Choy, R.L. Byer: Phys. Rev. B **14**, 1693 (1976)
35 C.K.N. Patel: Phys. Rev. Lett. **16**, 613 (1966)
36 I. Shoji, T. Kondo, A. Kitamoto, M. Shirane, R. Ito: J. Opt. Soc. Am. B **14**, 2268 (1997)
37 A. Szilagy, A. Hordvik, H. Schlossberg: J. Appl. Phys. **47**, 2025 (1976)
38 M.W. Sigrist, A. Bohren, I.G. Calasso, M. Nägele, A. Romann, M. Seiter: Proc. SPIE **4063**, 17 (2000)
39 I. Calasso, M.W. Sigrist: Rev. Sci. Instrum. **70**, 4569 (1999)
40 W. Meier-Augenstein: J. Chromat. A **842**, 351 (1999)
41 NIST: *Physical Reference Data*, http://physics.nist.gov/PhysRefData/contents.html
42 M. Nägele, M.W. Sigrist: Appl. Phys. B **70**, 895 (2000)
43 B.A. Paldus, T.G. Spence, R.N. Zare, J. Oomens, F.J.M. Harren, D.H. Parker, C. Gmachl, F. Capasso, D.L. Sivco, J.N. Baillargeon, A.L. Hutchinson, A.Y. Cho: Opt. Lett. **24**, 178 (1999)
44 A.A. Kosterev, F.K. Tittel, C. Gmachl, F. Capasso, D.L. Sivco, J.N. Baillargeon, A.L. Hutchinson, A.Y. Cho: Appl. Opt. **39**, 6866 (2000)
45 D. Hofstetter, M. Beck, J. Faist, M. Nägele, M.W. Sigrist: Opt. Lett. **26**, 887 (2001)